Coupling multitemporal remote sensing with geomorphology and hydrological modeling for post flood recovery in the Strymonas dammed river basin (Greece)

D. Capolongo[1a, 5e, *]

domenico.capolongo@uniba.it

A. Refice[2b]

D. Bocchiola[4d]

A. D'Addabbo[2b]

K. Vouvalidis[3c]

A. Soncini[4d]

M. Zingaro[1a]

F. Bovenga[2b]

L. Stamatopulos[3c]

[1a]Earth and Geoenvironmental Science Dept, University of Bari, Bari, Italy

[2b]Istituto per il Rilevamento Elettromagnetico dell'Ambiente (IREA), Consiglio Nazionale delle Ricerche (CNR), Bari, Italy

[3c]School of Geology, Aristotle University of Thessaloniki, Greece

[4d]Politecnico di Milano, Dept. ICA, P.za L. da Vinci 32, 20138 Milano, Italy

[5e]Dep. of Geology, University of Patras, University Campus, 26504, Rio Achaia, Patras, Greece

*Corresponding author.

Editor: Ralf Ludwig

Abstract

We present a case study of a long-term integrated monitoring of a flood event which affected part of the Strymonas dammed river basin, a transboundary river with source in Bulgaria, which flows then through Greece to the Aegean Sea. The event, which affected the floodplain downstream the Kerkini dam, started at the beginning of April 2015, due to heavy rain upstream of the monitored area, and lasted for several months, with some water pools still present at the beginning of September, due to the peculiar geomorphological conditions of the watershed. We collected a multi-temporal dataset consisting of a high-resolution, X-band COSMO-SkyMed, and several C-band Sentinel-1 SAR and optical Landsat-8 images of the area. The results allow following the event in time, sketching a multi-temporal map of the post-flood evolution, with relatively high temporal resolution. We then use hydrological modeling to mimic the dynamics of the flooded area against post event weather patterns and thus explain the observed flood extent evolution. We show how integrating remote sensing-derived maps of flooded areas, geomorphological analyses of the landscape and simplified hydrological modeling allows accurate inference about long-term dynamics of flooded areas, very important in the post event in anthropogenic highly modified areas, where recovery time after the flood event is considerable, and long term water persistence may lead to large consequences, carrying economic damages and medical emergencies.

Keywords: Flood; Geomorphology; Hydrological model; Multitemporal remote sensing; Strymonas river

1.1 Introduction

Research is recently exploring the integration of remote sensing, geomorphology and hydrological ~~modelling~~modeling for flood analyses (e.g. Refice et al., 2018a). One of the most common applications deals with the retrieval and mapping of inundation area extent and other flood hydrology information, since hydrological data collection is still considered a difficult task to date, in several basins around the world (Schumann et al., 2009, Refice et al., 2018b). Remote sensing, however, plays an important role in all the phases of hazard management, from the alert and preparedness phase to the emergency management and civil protection, up to damage assessment for risk reduction. Yet, it needs to be integrated with geomorphological knowledge of the area, to understand the spatial distribution of landforms and surface processes that can impact flooding events (Faccini et al., 2016, Righini & Surian, 2018).

Research and operational activities in the field of flood monitoring and prevention benefit from availability of both optical and radar remotely sensed (RS) data. RS data offer some long recognized advantages, such as the capability of providing synoptic information over wide areas at low costs, the reliability of data acquisition schedule, the immunity to local hindrances such as site accessibility or dangerous environmental conditions.

However, efficient flood monitoring through RS is a difficult problem, mainly due to the lack of data with sufficient acquisition frequency and timeliness (Grimaldi et al., 2016). This situation is worsened by the typically cloudy weather conditions associated with floods, which obstacle the propagation of e.m. waves in the optical spectral range, hampering acquisitions by optical sensors.

This problem is not present for longer (microwave) wavelengths, so that radar imaging sensors are recognized as viable solutions for reliable, multi-temporal flood event monitoring (Pulvirenti et al., 2014, Refice et al., 2014).

When available, RS information can be fruitfully used for the assessment and calibration of hydraulic flood models. For instance, Wood et al. (2016) used a long-term record of RS flood extents as calibration dataset of a hydraulic model. Further recent studies show that RS observation of both water level and flood extents can be used to calibrate state variables and parameters in the flood ~~modelling~~modeling practice (e.g. Matgen et al., 2015, 2016). These studies clearly show the value of RS datasets for improving hydrological/hydraulic models and the need for development of new methods and algorithms for a better integrated system. However, due to the usually fast dynamics of flood events, it is rarely possible to find sufficient numbers of RS acquisitions available to calibrate model parameters in a fully satisfactory way over a single event. Most often, images are available for different events on the same area (De Musso et al., 2018).

In this paper, we present a case study of long-term integrated monitoring of a flood event which affected part of the Strymonas dammed river basin, a transboundary river with source in Bulgaria, which flows then through Greece to the Aegean Sea. The event, which affected the floodplain close to the river mouth, started at the beginning of April 2015, due to heavy rain upstream of the monitored area, and lasted for several months, with some water pools still present at the beginning of September, due to the peculiar geomorphological conditions of the watershed. These conditions allow ~~to explore~~exploring the coupling of geomorphological analyses and hydrological ~~modelling~~modeling, with a quite large dataset of RS images to assess the post event phase in large flat or bowl shaped areas, where recovery time after the flood event is considerable, and long term water persistence is seen. We collected a multi-temporal dataset consisting of a high-resolution, X-band COSMO-SkyMed, and several C-band Sentinel-1 SAR, and optical Landsat-8 images of the area. The results allow following the event in time, sketching a multi-temporal map of the post-flood evolution, with relatively high temporal resolution. We then use the ~~*Pol*~~*Poly*-*Hydro* model (Soncini et al., 2017) to mimic the dynamics of the flooded area against post event weather patterns and thus explain the observed flood extent evolution. The ~~*Pol*~~*Poly*-*Hydro* model treats the flooded area as a reservoir, and uses input data on temperature and precipitation, water budget concepts, and simplified hydraulic modeling of stream and flood plain flow to track water surface, and outgoing water fluxes, so being able to represent slow post event flood dynamics. The base parameters of the model are here calibrated against flood extent data from the RS maps, and can be used henceforward for post event flood dynamics modeling in this area. The model parameters inferred from remote sensing allow to further increase the temporal modeling resolution, leading to a model of the basin draining with daily frequency. Although several of the remaining parameters are assigned through “educated guesses” or from rather general assumptions, the considerably realistic appearance of the final result, corroborated by in situ observations and site knowledge, demonstrates that RS data may act as a viable proxy for local discharge and other hydraulic information. This is important e.g. in the monitoring of remote basins, where no ground sensors (like gauges) are available.

~~2.~~2 Study area

~~2.1.~~2.1 Geographical and historical background

The Strymonas River (Struma River) is a transboundary river flowing through Greece and Bulgaria. Its drainage basin covers an area of 17,150 km^2. The greatest part of the basin (10,790 km^2) is located in Bulgaria, and small parts in FYROM and Serbia-Montenegro. The Greek part of the river drainage basin is divided in two: the Serres Basin, with an area of 3,970 km^2, drained by the Strymonas River, and the Drama Basin (2,385 km^2), drained by the Aggitis River, the main tributary of the Strymonas (Vouvalidis, 1998).

The Strymonas is a highly regulated river today. Before the extensive hydraulic works in the 1930’s, the geomorphology of the valley was totally different (Fig~~ure.~~ 1). In the northern part of the basin, close to the Greek-Bulgarian border, the Strymonas River reaches the lowland area of the Serres basin, passing through a gorge and an intra-mountainous route. On the entrance to the basin, an extensive, low inclination, alluvial fan was formed, with high avulsion rates of multiple braided channels (Fig~~ure.~~ 1, area 1). Between the alluvial fan at the NE, and the mountainous area at the NW, a temporal shallow lake and a marshy area was formed. This was a former lake, that after the dam construction is known as Kerkini Lake. The bottom of the lake had an elevation of +25 m a.s.l. while the mean lake level was at +29 m a.s.l. (Genidounias, 1935). Downstream of the Kerkini Lake, there were two main channels of the

Strymonas drainage network, parallel to each other. The first was the main channel of the Strymonas River, which was draining the central part of the plain and the hilly terrain of the western foothills of the valley. The other, on the east, was the Belitsa Torrent, that was draining the lofty terrain of Mount Menoikion. Both channels reached the Achinos Lake and formed small lake deltas at the northern part of the lake (Figure 1, areas 2 & 3). The Achinos Lake was a shallow elongated lake, that was morphologically divided in two due to the lake-delta progradation of Aggitis River (Figure 1, area 4). The bottom of the lake had a mean elevation of about +4 m a.s.l. (lowest at +3.22 m a.s.l.) while the level of the lake was ranging between +5 m a.s.l. to +8 m a.s.l., during dry and wet periods, respectively (Genidounias, 1935).

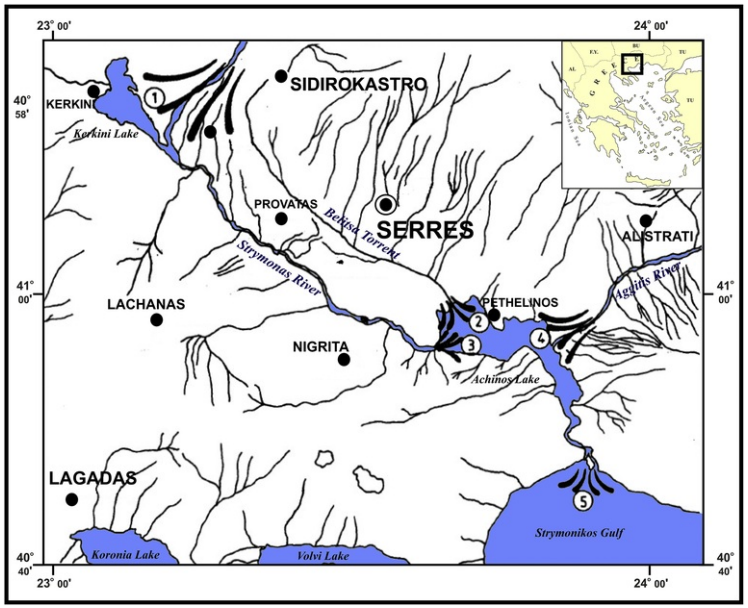

~~Figure 1.~~Fig. 1 Drainage network of the Strymonas River, the Kerkini and Achinos Lakes and the fluvial deposition areas in the valley before human intervention and river regulation in the 1930~~-~~s. (1) Alluvial Fan, (2), (3) & (4) Lake Deltas, (5) Strymonas River Delta.

alt-text: Fig. 1

~~2.2.~~2.2 Geomorphological and hydrological setting

The present day morphology and hydrology of the plain is completely different from the natural one before the hydraulic works in ~~1930~~the 1930s. Nowadays, the channel of the Strymonas River is highly regulated by the construction of levees, weirs and dredging along its main channel. Also, a dam construction with a peripheral embankment, in a low laying area in the NW part of Serres basin (Figure 1, area 1) is responsible for the creation of a shallow (3~~-~~7 m deep) lake reservoir (Figure 2). Very soon after the reservoir construction, the Strymonas River developed a delta in the Kerkini Reservoir, where a very important wetland was established, protected by the RAMSAR convention for “Wetlands of International Importance” (Matthews, 1993). Since then, ordinary people forgot the artificial character of the system, which is now known as Kerkini Lake. Downstream the Kerkini Lake dam reservoir, the channel of the Strymonas River is confined between levees, while the channel of the Belitsa Torrent has been dredged in order to support higher discharges of fluvial runoff coming from Mount Menikion. The channel-bottom slopes in both channels have been regulated by weirs in order to avoid channel incision and knick-point migration due to the drainage of the Achinos Lake and the decline of the base level. The Achinos Lake was drained by the construction of a new channel, by dredging the bottom of the lake. The construction of a deep channel, confined by levees, along the bottom of the drained lake failed quite soon, due to the unstable fine sediments of the lake bottom that were responsible for levee subsidence and channel instability. This channel morphology is responsible for the discharge of the channel at bankfull stage in the entire drainage system of the Strymonas River. As mentioned, the major part of the basin (10,790 km^2) is located outside Greece. This implies that the major flood events that happen between the borders and the Kerkini Lake (dam reservoir) Impact the channel segment of the Strymonas River. An artificial channel with levees was constructed between the Bulgarian borders and the artificial Kerkini Lake. The maximum channel discharge was 3~~,~~000 m^3~~/sec~~s. Today, due to sediment deposition along the channel, the maximum discharge ranges between 1~~,~~200 and 1~~,~~500 m^3~~/sec~~s. Downstream the Kerkini reservoir, the Strymonas channel was constructed for a maximum discharge of 700 m^3~~/sec~~s. In the channel segment of the Strymonas River on the southern part of the old drained Achinos Lake (Figure 2), just after its junction with the Aggitis River, the maximum discharge Q_{Th} is ~~less than~~ ≤200 m^3~~/sec~~s. The width of the channel is ~80 to 100 m, its depth ranges between 2~~ to~~ and 3 m, and the slope is ~~less than~~ ≤1‰, without side embankments. All the fluvial system is regulated by the Kerkini dam. The regulated dam outflow depends on runoff conditions of Serres and Drama Basins.

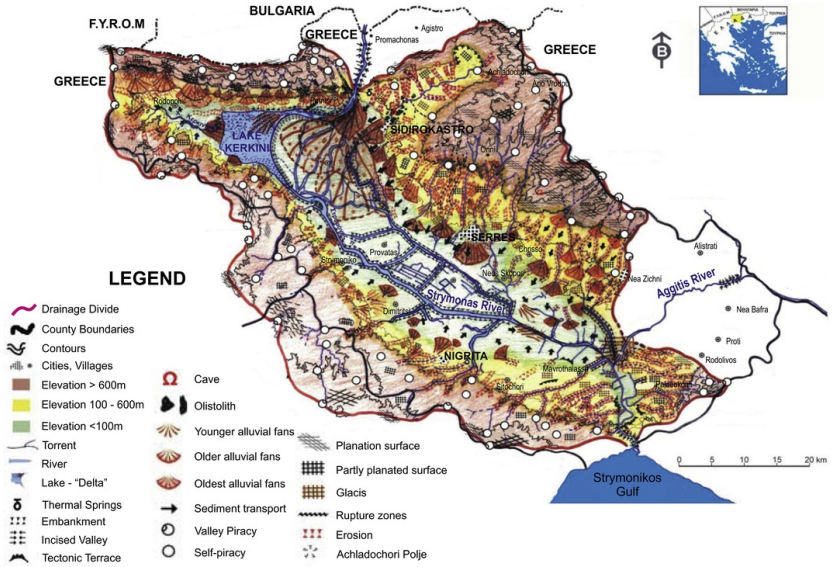

~~Figure 2.~~Fig. 2 Present geomorphology of the lower part of Strymonas Basin (Serres plain)~~.~~

~~(~~*Modified after Papafilippou-Pennou ~~[~~2004~~]~~*~~).~~

alt-text: Fig. 2

The larger the fluvial runoff downstream the reservoir, due to local precipitation conditions, the lower the dam outflow. The Kerkini reservoir is used as a buffer volume for the hydrological regulation of the river discharge that shouldn~~'~~t exceed the total value of 200 m^3 ~~/sec~~s in the Achinos drained Lake channel segment. This is for maintaining the channel flow conditions in this segment at bankfull stage. The worst hydrological scenario is a simultaneous flood event in the Strymonas basin, both upstream and downstream the Kerkini Lake reservoir. In this case, the dam outflow is regulated due to the available reservoir capacity at that specific time and the upstream water discharge of the river. This regulation is essential for the dam protection; even the local authorities know that the lower part of the basin will be flooded. This situation was seen occurring every 10 to 20 years.

The water volume in the Kerkini reservoir fluctuates during the year. Usually during winter is at the lowest level, in order to regulate the river floods, but in late spring (end of May) the lake is full, using the water for irrigation purposes during summer.

~~3.~~3 Data and ~~M~~method

~~3.1.~~3.1 Geomorphological data

In order to compare the flood effects with the main geomorphological features of the area of interest, we georeferenced historical maps and analyzed them in conjunction with a Digital elevation model. These maps are operational topographic maps with a scale of 1:100,000, initially produced by the Greek Geographical Military Service in the 1930~~'~~s, and reprinted by the German army during WWII. These maps were not fully updated in all sheets, but still allow ~~to recognize~~recognizing the geomorphological features of the Achinos Lake (shoreline, lake-deltas marshes, reeds etc.). ~~This~~ These geomorphological features have been mapped to produce the geomorphological map of Fig~~ure.~~ 2.

We then used the digital elevation data from the JAXA Global World DEM, with a 30 m-pixel posting, to derive water levels at different time steps from the remotely sensed data, and as base topographic data to apply the hydrological model. Also, daily temperature and precipitation data were extracted for the Serres station from the Greek Meteorological Service database, covering the period April 1st to September 30th, 2015.

~~3.2.~~3.2 Remote sensing data

Several images, both optical (Landsat 8) and SAR (Sentinel-1 and COSMO-SkyMed) were used to map inundated areas at different times during and after the flood event. Table 1 reports the main characteristics of the used data. In the table, image dates and times are reported in temporal sequence. Note the availability of both SAR and optical data on the date of 04/04/2015, although acquired at different times. The L8 image acquired in February shows

no sign of flood, and has been used to derive the *thalweg* morphology and "normal" river streamflow. SAR images were absolutely calibrated. Then, they were speckle-filtered through a filter based on a nonlocal paradigm (Deledalle et al., 2015), which has been shown to smooth out homogeneous regions, while retaining high resolution over terrain features causing sharp signal variations, such as man-made point-like or linear features, or, more appropriately, the sharp edges between water and dry areas. The speckle-filtered backscattering coefficient (σ^0) images were then precisely geocoded through the range-doppler algorithm (Schreier, 1993); optical images were radiometrically corrected to obtain ground reflectance values (Chander and Markham, 2003). Then, both SAR and optical images were resampled to a common grid with 10 m spacing in both directions. NDVI maps were derived from optical images, defined pixelwise as ($\rho_{NIR-}\rho_R/\rho_{NIR+}\rho_R$), where ρ_{NIR} and ρ_R are the reflectance in the near infrared and red bands, respectively. A buffer zone, largely encircling the maximum extent of the flooded area, was considered around the river course, and values within such area were analyzed (see Refice et al., 2018c).

~~**Table 1.**~~**Table 1** List of remotely sensed data, acquisition dates and times. L8 = Landsat 8, CSK = COSMO-SkyMed, S1 = Sentinel-1. Asterisks denote partial coverage of the region of interest due to cloud presence, which however does not affect flooded area estimation.

alt-text: Table 1

Sensor	Date	Time	
L8	15/02/2015	09:04:08	
CSK	01/04/2015	16:11:07	
S1	04/04/2015	04:30:34	
L8	04/04/2015	09:03:42	
S1	16/04/2015	04:30:23	
S1	28/04/2015	04:30:24	
L8	06/05/2015	09:03:28	
S1	22/05/2015	04:30:25	
L8	14/06/2015	09:09:47	*
L8	23/06/2015	09:03:39	
L8	09/07/2015	09:03:49	
L8	16/07/2015	09:10:04	*
L8	25/07/2015	09:03:56	
L8	01/08/2015	09:10:08	*
L8	10/08/2015	09:03:59	
L8	02/09/2015	09:10:19	*
S1	07/09/2015	04:30:32	
L8	11/09/2015	09:04:14	
L8	18/09/2015	09:10:28	*

Both SAR backscatter and optical NDVI are expected to be low on smooth water areas, as both microwave and optical radiation is, in this case, mostly reflected in the specular direction, which in both cases points away from the receiving sensor. A simple means to separate water and land areas consists thus in applying a threshold to each image in the dataset. In our case, restricting the attention to the above-mentioned buffer zone eliminates potential problems connected with the different size of populations of flooded vs. non-flooded image pixels, as well as to the occurrence of other changes than the flood. We then used a single threshold value for all the SAR and a single value for all the optical images. The threshold values were derived by comparing the optical and SAR images acquired on the same date, i.e. on April 4th, 2015. Assuming the ground truth to be practically the same for both these two acquisitions, we seek the threshold values around the histogram minima which maximize the agreement between the flood maps obtained by the two sensors. In practice, we consider a grid of threshold value pairs, spanning intervals

between −15 and −7 dB with a step of 0.1 dB, for SAR, and between −0.1 and 0.1 with a step of 0.005, for the NDVI. For each pair of thresholds, we compare the SAR and the optical binary flood map and compute a merit figure, given by Cohen's K value (Cohen, 1960), to determine their agreement. We then use the above-mentioned pair of thresholds corresponding to the maximum K value to derive binary maps for each date.

Further details of the processing can be found in Refice et al. (2018c). The output of the procedure is a sequence of binary maps, one for each date, where flooded pixels are assigned the value 1, and non-flooded pixels, 0.

~~3.3.~~3.3 Hydrological ~~modelling~~modeling

A hydrologically based modeling tool, the Poli-Hydro model, was used in the data analysis phase, to mimic the emptying of the Strymonas lake. Poli-Hydro is a semi-distributed hydrological model based upon simplified water budget equations, developed at Politecnico di Milano, suitable to represent the hydrological cycle of catchments within a large spectrum of climatic and hydrologic conditions. The tool works on meso-scale to micro-scale, high altitude, snow/ice fed catchments, also in arid and semi-arid areas, as well as in tropical climates (Bocchiola et al., 2010; Groppelli et al., 2011; Migliavacca et al., 2015; Bozza et al., 2016; Soncini et al., 2016, 2017).

In our case, given the mostly flat morphology of the flooded area, and its slow post-event emptying phase, dynamic effects (i.e. 2-D flow velocity within the flooded domain) can be neglected with little loss of accuracy, and the area can be basically represented as a still water surface (a pond, or a reservoir), so that the dominant processes are those used in standard approaches to hydrological budgets, namely precipitation and inflows (as inputs), evapotranspiration and soil infiltration (as outputs). The model tracks variation of water content in soil within the dry area (not flooded) of the catchment, W_S [mm], and in the lake, V_L [m^3], in two successive time steps (t, $t+\Delta t$) as:

$$\begin{aligned} W_S(t+\Delta t) &= W_S(t) + R\Delta t - ET\Delta t - Q\Delta t; \\ V_L(t+\Delta t) &= V_L(t) + V_f(t) + A_L R_L \Delta t + A_B Q_G \Delta t \\ &+ A_B Q_S \Delta t - A_L ET_L \Delta t - A_L Q_{GL} \Delta t - A_L Q_{SL} \Delta t. \end{aligned} \quad (1)$$

Here a daily time step Δt is used, R [mm d^{-1}] is the liquid rain, ET [mm d^{-1}] is the actual evapotranspiration on the dry area. Q [mm d^{-1}] is the discharge from the catchment assumed to reach the lake moving towards the river, and includes both the subsurface and overland flow contributions from the drainage area. In the second equation, V_f [m^3] is the flooding volume, A_L is the lake area [km^2], R_L is the liquid rain on the lake area, ET_L [mm d^{-1}] is the actual evapotranspiration on the lake (taken equal to the potential evapotranspiration, ETP), and Q_{GL} [mm d^{-1}] is the infiltration discharge under the lake (for a soil always saturated in the presence of flooding). Potential evapotranspiration is calculated here using Hargreaves' equation, requiring only temperature data (and water equivalent of solar radiation, in mm). Overland flow on land Q_S occurs for saturated soil above a maximum content W_{Max} [mm].

$$Q_S = \begin{cases} W(t+\Delta t) - W_{\mathrm{Max}} & \text{if } W(t+\Delta t) > W_{\mathrm{Max}}; \\ 0 & \text{if } W(t+\Delta t) \le W_{\mathrm{Max}} \end{cases} \quad (2)$$

Overland flow outside the lake (i.e. water flowing above the threshold level of catchment closure h_{Th}, and going towards the sea) Q_{SL} can be modeled according to a reservoir scheme as

$$Q_{SL}(t) = \begin{cases} C\left(h(t) - h_{Th}\right)^{\alpha} = \frac{1}{T_l}\left(h(t) - h_{Th}\right)^{\alpha} & \text{if } h(t) > h_{Th}; \\ 0 & \text{if } h(t) \le h_{Th}, \end{cases} \quad (3)$$

with α reservoir exponent, and T_l [mm$^{\alpha-1}$ d] lag time of the reservoir. Here we used $\alpha = 1$, i.e. a linear reservoir approach, for simplicity. Accordingly, overflow from the catchment is linearly related with water volume within the flooded area (above the h_{Th} level). In analogy with lumped hydrological modeling taking the catchment as a linear reservoir with a given Instantaneous Unit Hydrograph (IUH), we assumed that T_l of the reservoir may be estimated as the ratio of the reservoir length (here matching with the main channel length), and a characteristic flow velocity within the reservoir, $T_l = L_{mc}/U_{re}$ (Bocchiola et al., 2003; Bocchiola and Rosso, 2009). We took $U_{re} = 1$ m s^{-1}, a plausible value from literature, and in analogy with in channel flow at maximum conveyance U_{ch}, explained below. During our case study flood event, the water level within the Strymonas depression did not reach the threshold value h_{Th}. Accordingly, the assumption of $U_{re} = 1$ ms^{-1} does not affect the proposed results for this specific flood event, but may be relevant whenever h_{Th} was exceeded. Lake area and volume change are linked to water depth in the lake, according to topographically assessed relationships, as:

$$\begin{aligned} h_L(t) &= f\left(W_L(t)\right); \\ A_L(t) &= f'\left(h_L(t)\right). \end{aligned} \quad (4)$$

Groundwater discharge (i.e. sub-superficial flow) in dry areas is expressed as a function of soil hydraulic conductivity and soil water content:

$$Q_G(t) = K_h W(t), \quad (5)$$

with K_h [mm d^{-1}] saturated horizontal permeability. Groundwater infiltration under the lake is expressed as a function of water depth h_L (hydraulic head), and soil vertical permeability as:

$$Q_{GL}(t) = K_v h_L(t). \quad (6)$$

Notice that we chose infiltration and sub-superficial flow linear with water depth and soil moisture, respectively. Albeit other choices were possible (i.e. by assuming non-linear dependence), here, given the lack of information about hydrological soil behavior (i.e. in the absence of information about e.g. hydrograph shape during recession periods), and in general to keep the number of tuning parameters low, we decided to assume linear behavior.

Stream flow discharge Q_R [$m^3 s^{-1}$] is calculated as a function of river stage h_R with Strickler's rule as

$$Q_R(t) = k_s h_R(t)^{5/3} \sqrt{sl} B \quad (7)$$

with k_s Strickler's coefficient [$m^{1/3} s^{-1}$], sl channel bed slope, B channel width. Strickler's coefficient is here estimated by back calculation of Equation (7), taking the values of geometric parameters B and sl from our DTM, and maximum in-channel conveyance $Q_{Th} = 200\ m^3 s^{-1}$. Calculation of flow velocity at maximum flow gave $U_{ch} = 1\ ms^{-1}$. This velocity could be used as a first approximation for U_{re} for calculation of T_l in Equation (3) as reported above. Overflow of the river levees (i.e. flooding of the Strymonas flatland) occurs as levee height is exceeded ($h_R(t) > h_{\text{levee}}$), as:

$$V_f(t) = \Delta t \left(Q_R(t) - Q_{Th}\left(h_{\text{levee}}\right) \right) \quad (8)$$

with Q_{Th} [$m^3 s^{-1}$] maximum in-stream conveyance, and V_f flooding volume used in Eq. (1). Eventually, the parameters left for model tuning are K_h, K_v, and W_{Max}. These three parameters were used to manually tune the model, and iteratively modified until a proper modeling of the flooded area was attained, i.e. by visual comparison against estimated flooded area from RS images.

4.4 Results and discussions

The sequence of binary images showing the water extent, derived from the RS data, constitutes in fact a rather peculiar database. The time evolution of the flooded area can be followed throughout the image sequence.

Fig. 3 shows a combination of all the binary maps starting from the L8 image acquired on April 4, which shows the greatest extent of flooded area. Such combined map is obtained by simply summing up the 1/0 binary images of each date, thus assigning increasing indices to pixels being inundated in increasing numbers of dates with respect to the total time series. Relying on the hypothesis of "monotonic" drainage, it is possible to note how peripheral areas are reached by the flood wave only for the day corresponding to the flood maximum, while some pixels, closer to the river course, stay flooded for most of the investigated dates, forming probably ponds which take long times to absorb or evaporate.

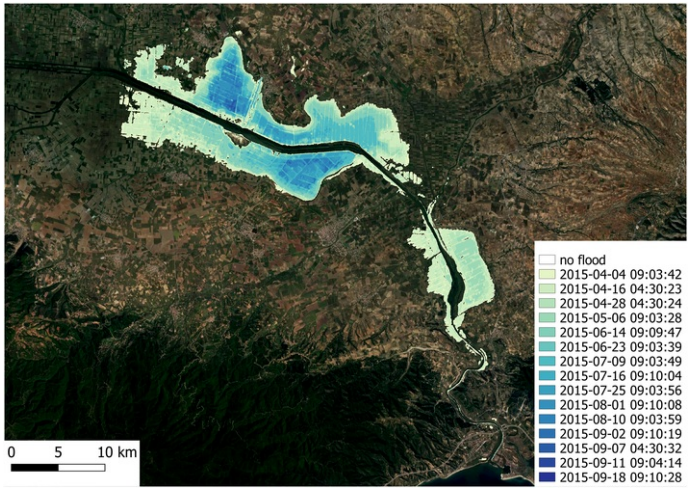

Figure 3.Fig. 3 Multi-temporal flood map from remotely sensed data. Assuming a temporally steady draining process, deeper blue in the colorcolour scale indicates pixels flooded for increasing time intervals, from the starting date of April 4, 2015 at 9:30 a.m. date of the first L8 image acquisition. (For interpretation of the references to colour in this figure legend, the reader is referred to the web version of this article.)

Background is from Google Earth®.

alt-text: Fig. 3

Besides its visual impact, this multi-temporal map can be used to infer some further geomorphological information about the event. Figure 4 shows a superposition of the RS-derived multi-temporal map in Figure 3 and georeferenced historical maps. This combination shows that the flood event of late March 2015 created a new water body in the area of the drained Achinos Lake, in the lower part of the Serres basin. The volume of the accumulated water was so large that it created a temporary lake, with maximum volume and surface more or less equal to those of the natural lake that existed in the area until the 1930s. The water covered not only the bottom of the drained natural lake, but also part of the areas that used to be the lake-deltas of the Strymonas and Belitsa Rivers, as well as the lakeside marshes and reeds. Geomorphological evidence that the surface of accumulated flood water reached an

altitude equal to the maximum level of the natural lake surface is provided by the proximity of the temporary lake shore to the Pethelinos Village. The Pethelinos Village was historically sited at the lakeside of the former natural Achinos Lake. The flood water approached the old lakefront of the village but the old houses remained unaffected by the water. The water did not cover areas that were the lake-delta of the Aggitis River in the natural lake, as it was expected. Therefore, it is reasonable to assume that the water surface level of the temporary lake was between +7 and +8 m a.s.l., which correspond to the maximum height of the former lake. The duration of the water permanence was longer than expected, because of two reasons. First of all, the absence of stream channel maintenance during the last decades allowed lateral torrents to deposit coarse material in the main channel, creating subsurface dams, reducing the cross section of the river channel and consequently the discharge at the bankfull stage. In addition, the flood event has compromised for a long period the pumping stations present in the Pethelinos area.

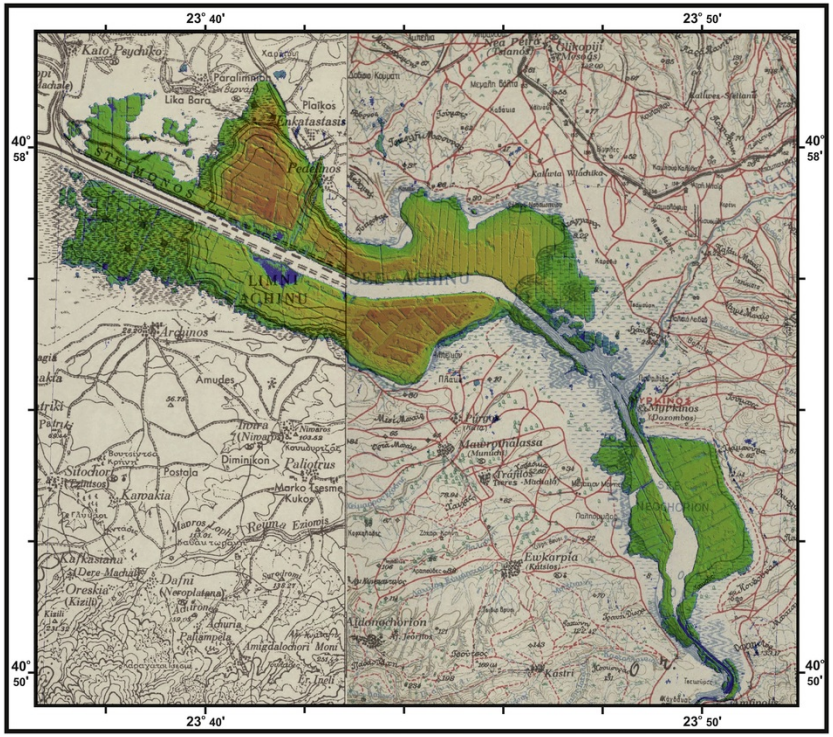

~~Figure 4.~~**Fig. 4** Extent of the 2015 flood area in relation to the 1930 topography (before the intense construction works). Orange colors represent the higher water level. (For interpretation of the references to colour in this figure legend, the reader is referred to the web version of this article.)

alt-text: Fig. 4

The area occupied by flooded pixels at each date in the region of interest can be computed and plotted in a graph, showing its evolution in time. Such plot is shown in Fig~~ure~~. 5. The trend of this plot shows a relatively sharp increase of the total flooded area, from around zero in February, up to a maximum of ~~more than~~ ≥6500 ha. (See Fig. 6.)

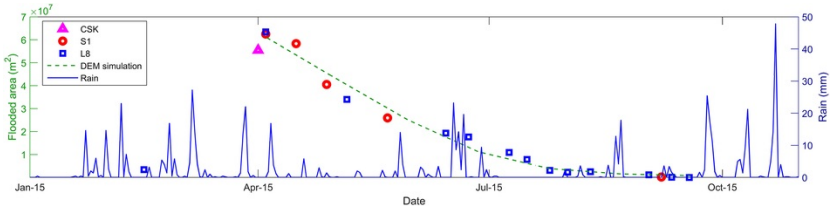

~~Figure 5.~~**Fig. 5** Temporal trend of the flooded area as deduced from the RS data. The dashed line refers to the simulation using the DEM described in the text.

alt-text: Fig. 5

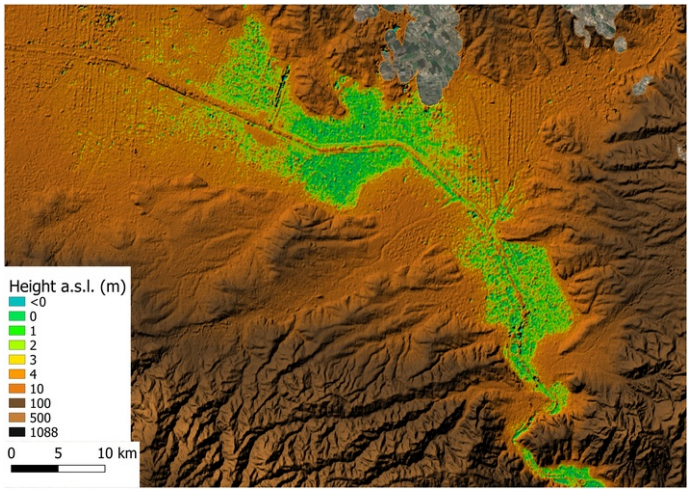

~~Figure 6.~~Fig. 6 ASTER DEM height map (© JAXA) draped on an optical image (© Google).

alt-text: Fig. 6

We used data from the JAXA Global World DEM to depict and reproduce different steps of the flood event dynamics. Figure 6shows the DEM height map. Missing data are visible in the upper part of the area, but the missing locations do not contribute to the flood area computation. Note, instead, the increased height recorded along the river course, which denotes the presence of elevated river levees. This is confirmed by close inspection of optical images. It can be noticed how the lowland area in the DEM map (green, yellow and light brown areas) appears similar in shape to the maximum inundated area as visible from the SAR S1 and optical L8 images. This area also corresponds to the ancient Achinos Lake shorelines.

We could then hypothesize that the flood phenomenon could be ~~modelled~~modeled as a simple spill of water from the river course onto the surrounding lowland, which then dried in time at a constant rate, as done in Refice et al. (2018c): we determined first the most likely height level reached by water, by deriving an optimal height level from the ROC curve obtained by varying the height threshold and using the maximum flood extent binary map as score; then, we simulated a progressive, steady decrease of the water level, linearly in time from the date of the maximum extent (April 4), to the end of the monitoring (Sept 2015), computing the total extents of the DEM area below each decreasing threshold. The resulting curve is plotted as a dashed green line in Fig~~ure.~~ 5. As can be seen, the overall agreement of the two trends is rather good, despite the RS data show several oscillations with respect to the model.

To gain further insight into the hydrological processes guiding the dynamics of the inundation, we subsequently applied the *Poli-Hydro* model (whose operational scheme is graphically represented in Fig~~ure.~~ 7). In Fig~~ure.~~ 8 we report the results of our modeling exercise. In Table 2 we report the model parameters, including those inferred by tuning against the RS data. Discharge in outflow from the dam Q_{Rel} (which filled the area, at least initially) was unknown, and accordingly we had to provide an estimation of such value based upon available information.

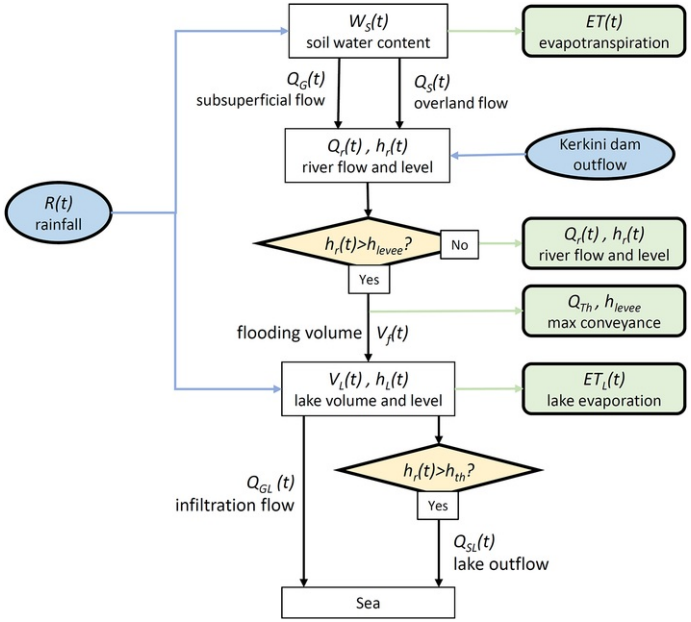

~~Figure 7.~~Fig. 7 Scheme of the *Poly-Hydro* model as applied to the present test case. Time t is in days. $W_S(t)$ is soil water content, $V_f(t)$ is the flooding volume from the Strymonas river, $V_L(t)$ is water volume in the flooded area (lake), $Q_r(t)$ is river flow, $Q_G(t)$ is subsuperficial flow from the catchment, $Q_S(t)$ is overland flow from the catchment, Q_{GL} water infiltration flow in the lake, $Q_{SL}(t)$ is outflow from the lake, Q_{Th} is maximum river conveyance, R is rainfall, ET is evapotranspiration from the catchment, ET_L is evaporation from the lake, $h_r(t)$ is water level in the river, h_{levee} is levee height, $h_L(t)$ is lake water level, h_{th} is threshold height for outflow from the lake.

alt-text: Fig. 7

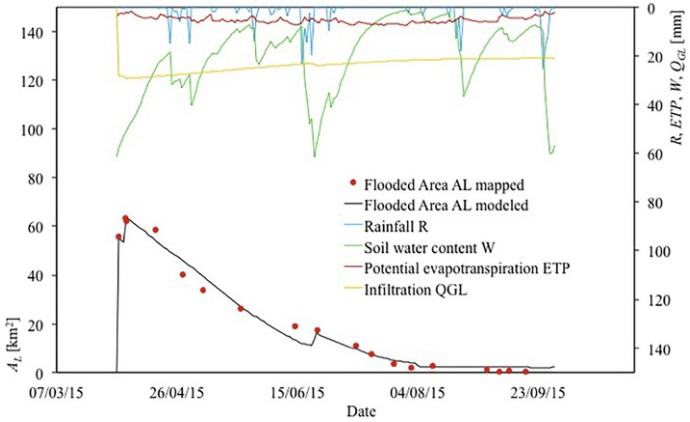

~~Figure 8.~~Fig. 8 Bottom black curve and red dots represent the temporal trend of the model-simulated flooded area and the flooded area observed by remote sensing, respectively (left vertical axis). Top colored curves represent rainfall R (blue), as well as other simulated quantities such as potential evapotranspiration ETP (red), soil moisture W (green), and groundwater infiltration Q_{GL} (yellow). They are referred to the right vertical axis (reversed). (For interpretation of the references to colour in this figure legend, the reader is referred to the web version of this article.)

alt-text: Fig. 8

Table 2 ~~Poli~~Poly-Hydro model. Model parameters calibration for the Strymonas River. Estimation mode explained here, and in the text.

alt-text: Table 2

Parameter	Unit	Description	Typical range	Value	Estimation mode
k_s	[$m^{1/3}\ s^{-1}$]	Stricklers' coefficient	1–100	20	Max in channel flow $Q_{Th} = 200\ m^3\ s^{-1}$
T_l	[d]	Reservoirs' characteristic time coefficient	>0	0.91	$T_l = L_{mc}/U_{re}$
α	[.]	Reservoir flow exponent	0.5–1.5	1	Linear reservoir
$K_{h,v}$	[mm d^{-1}]	Saturated conductivity, horizontal, vertical	>0	1.7, 0.25	Tuning vs. flood area
W_{Max}	[mm]	Max soil storage based on SCS-CN method	0–2300	62	Tuning vs. flood area
θ_w, θ_s	[.]	Water content, wilting, field capacity	$0 < \theta_w, \theta_s < 1$ $\theta_s > \theta_w$	0.15, 0.35	Literature

We reasonably hypothesized that a large release had occurred from the dam in those days when the pool level in the flooding area rose, and no rainfall occurred to justify such increase. From Figure 8, this would have occurred at least on two occasions. First, on April 1st (i.e. when the first flood image is collected from COSMO-SkyMed), with an outflow from the Kerkini dam estimated to peak at $Q_{Rel} = 1000\ m^3\ s^{-1}$, exceeding largely the stream conveyance, estimated roughly into $Q_{Th} = 200\ m^3\ s^{-1}$ as reported in Equation (7). A second event may have occurred around April 4th ($Q_{Rel} = 500\ m^3\ s^{-1}$) when clearly water level rose in the pond without any significant precipitation having occurred. Such values of Q_{Rel} are clearly mere estimations based upon the observed flooded area, and other unknown processes may have occurred therein. Further hydrological information could improve model results. Notice that in other dates we set $Q_{Rel} = 0$, basically meaning that no over flooding occurred, which instead occurs when $Q_{Rel} > 200\ m^3\ s^{-1}$.

Maximum soil moisture W_{Max} was unknown, as reported, and was calibrated against estimates of flooded area from RS data, so being the first model tuning parameters used here. The result is acceptable given the nature of the local soil, mostly covered in vegetation.

Initial (i.e. on day April 1st) soil moisture W_0 was set to W_{Max} (i.e. saturated soil), likely after the flood event. The dynamics of W_{Max} on dry land (being $W = W_{Max}$ in the flooded area) is also reported in Figure 8. Visibly, increase of flooded area occurs when $W = W_{Max}$ given that overland flow Q_S occurs at soil saturation (Equation 2), and increases the impounded volume (Equation 1). This happened around June 22nd, in the wake of large precipitation (with a max of 23 mm on June 17th and more rainfall after that).

Saturated permeability, horizontal, and vertical $K_{h,v}$ [mm d^{-1}] to be used in Equation (5) and Equation (6) are the other two model tuning parameters here. They are basically estimated by visual fitting of the magnitude and shape of the decreasing limbs of the pond's area A_L vs date (approx. April 6th–June 26th), which is clearly dominated by infiltration processes (Q_G, Q_{GL}), during dry spells (i.e. when neither precipitation, nor overflow occurs). We chose here Eqs. (5) and (6) to keep both infiltration and sub-superficial flow linear with water depth, and soil moisture, respectively. Albeit other choices were possible (i.e. by assuming nonlinear dependence), given the lack of information about hydrological soil behavior (e.g. in the absence of information about hydrograph shape during recession periods), we decided to keep this linear relation for simplicity, and also to reduce the number of model's parameters (i.e. to avoid assessment of two exponents).

In our modeling exercise in practice no water flows occurred outside of the ponded area (Q_{SL} in Eq. 3), given that the maximum flow level remained mostly below 4 m a.s.l., which is the approximate threshold for basin closure h_{Th} in Eq. (3), as also seen clearly in Figure Fig. 8. As a reference, flow outside the pond would have occurred in case a larger outflow would have occurred from the dam. Here, as a mere example, if the dam's outflow would have been of ~1500 $m^3\ s^{-1}$ (instead of 1000 as calculated above) upon April 1st, and again 500 $m^3\ s^{-1}$ like estimated here upon April 4th this would have risen the pond level up to ca. 4.03 m a.s.l., slightly above the threshold for overflowing. However, such level would have corresponded to a flooded area of ca. $A_L \sim 76.4\ km^2$ upon April 4th, instead of $A_L \sim 62\ km^2$, as estimated here, so we can assume confidently enough that such level was not reached during our period of study.

Given the obviously limited number of images available, we tuned the model manually based upon visual fitting of the flooded areas, and we made no endeavor into automatic model tuning (i.e. assessment of the three chosen tuning parameters here W_{Max}, $K_{h,v}$) based upon minimization (maximization) of objective indexes (e.g. using systematic error bias, or Nash Sutcliffe Efficiency). Such exercise may be left for future developments, when other events might be studied, so obtaining some redundancy for robust (semi-) automatic model estimation.

Notice that when introducing an increasing number of parameters, model tuning based upon the sole flood extension may be ill-posed, also considering the uncertainty connected with assessment of the flood extent, i.e. of the flow release from the Kerkini dam. Accordingly, before any refined objective tuning procedure is attempted, more information is required, to constrain the model parameters more tightly.

As an example, the parameter W_{Max} may be estimated via e.g. land use classification based on the SCS-CN method (Soncini et al., 2016), and/or via soil sampling. Similarly, soil permeability may be measured with soil sampling, and infiltration tests. Also potential evaporation *ETP*, here modeled according to Heargraves' method, may be measured, say, with evaporation pans. Even stream flow conveyance Q_{Th} was posed from reasonable assumptions here, but validation is needed, maybe based upon historical data of flow measurements therein, or even upon new measurements.

With all these caveats, one sees from Figure 8that our simple, manually tuned model is capable of simulating decently the dynamic of the pond, during i) the flooding phase (approx. April 1st–5th), however linked to the initial hypothesis on Q_{Rel}, ii) the emptying phase (approx. April 6th–June 22th), when rainfall is not enough to offset evapotranspiration, and infiltration, and iii) the secondary filling phase (on June 22rd–23rd), when precipitation saturates the soil ($W = W_{Max}$), and produces superficial runoff, contributing to the further, small lake level increase.

Accordingly, the proposed model and the adopted parameters represent a preliminary approach to demonstrate the feasibility of our objectives, i.e. i) simulation of the inundated area in time, and ii) description of the main hydrological fluxes governing the flooding phenomena. Our proposed hydrological model integrated with RS data can thus mimic reasonably well the post flood dynamics of the area.

5.5 Conclusions

We show how integrating remote sensing-derived maps of flooded areas, geomorphological analyses of the landscape and simplified hydrological modeling allows accurate inference about long-term dynamics (i.e., in this case, the slow emptying of a reservoir) of flooded areas, very important in the post event phase in large flat or bowl-shaped areas, where recovery time after the flood event is considerable, and long term water persistence may lead to large consequences, carrying economic damages, and medical emergencies.

We found that the final spatial distribution of the inundated areas, relevant to the inundation event occurred in late March 2015 on the Greek part of the Strymonas river floodplain, was strongly controlled by the geomorphological history of the river basin whose former configuration, before the 1930s heavy construction works, was the main factor to drive the final spatial distribution of the flood, and the main reason of its long persistence in the landscape. In fact, most of the inundated areas correspond to the surface occupied by the old Achinos Lake. Furthermore, the new channel constructed after the ~~1930~~1930s, with levees higher than the actual flood plain, prevented the easy outflow of the water, so that the draining of the area was due mainly to evaporation and infiltration processes.

This particular geomorphological setting is an ideal situation, not very common, to use hydrological modeling and remote sensing maps to assess the post flood dynamics.

Usually, in fact, due to the velocity of flood dynamics, models based on the propagation of the shallow equations cannot be easily calibrated/validated with remote sensing data, due to the scarcity of the latter due to low frequency of acquisition, in turn mainly due to cloud cover conditions for optical data. In our case, this is partially overcome thanks to the rather dry climate settings of the studied area during the post-flood phase, and by the use of SAR images, not affected by cloud cover. Furthermore, our case study presented a slow dynamics, which allowed collecting an unusually extensive RS dataset covering the event, coupled with an hydrological setting in which evaporation and infiltration processes predominate. For the above geomorphological reasons, the post flood recovery and dynamics was mainly a problem of hydrological balance, rather than a dynamic problem. This was therefore an ideal natural experiment to derive several inundation maps at different time steps that depict the spatial evolution of the inundation. Those maps constitute a sufficient, and usually not available dataset to be used to calibrate and validate the parameters and the results of the hydrological model.

We use the stacks of inundation maps to estimate the saturated conductivity of the soil and the maximum soil capacity storage. At the time of the study, the discharge in outflow from the dam was unknown and had to be estimated, but in the future this could be a known parameter that could improve the performance of the model.

In the same way, applying this methodology to future flood events will help to evaluate the stability of the hydrological parameters for a model application in the sense of flood dynamics modeling based on short to medium term meteorological forecast, and informed management of post flood recovery activities.

Uncited references

Bocchiola et al., 2011

Rinaldo et al., 2012

Acknowledgements

We thank the anonymous referees for their helpful comments. COSMO-SkyMed imagery is provided by ASI (Agenzia Spaziale Italiana) in the framework of the COSMO-SkyMed/RADARSAT-2 Joint AO project “Spectral and temporal coherence for vessel detection and flood monitoring” (ID 2888/5229). DEM data © Japan Aerospace Exploration Agency (JAXA).

References

Bocchiola D. and Rosso R., Use of a derived distribution approach for extreme floods design: a case study in Italy, *Adv. Water Resour.* **32** (8), 2009, 1284–1296.

Bocchiola D., De Michele C., Pecora ~~S~~S. and Rosso R., Sul tempo di risposta dei bacini idrografici italiani. [On the Response Time of Italian Watersheds], L'ACQUA, **vol. 1**, 2003, 45–55, (In Italian with abstract in English).

Bocchiola D., Mihalcea C., Diolaiuti G., Mosconi B., Smiraglia C. and Rosso R., Flow prediction in high altitude ungauged catchments: a case study in the Italian Alps (Pantano Basin, Adamello Group), ~~*Advances in Water Resources*~~*Adv. Water Resour.* **33**, 2010, 1224–1234.

Bocchiola D., Diolaiuti G., Soncini A., Mihalcea C., D'Agata C., Mayer C., Lambrecht A., Rosso R. and Smiraglia C., Prediction of future hydrological regimes in poorly gauged high altitude basins: the case study of the upper Indus, Pakistan, *Hydrol. Earth Syst. Sci.* **15**, 2011, 2059–2075.

Bozza A., Durand A., Confortola G., Allenbach B. and Bocchiola D., Potential of remote sensing and open street data for flood mapping in poorly gauged areas: a case study in Gonaives, Haiti, *Applied Geomatics* 2016, 1–15, https://doi.org/10.1007/s12518-016-0171-x.

Chander G. and Markham B., Revised landsat-5 tm radiometric calibration procedures and postcalibration dynamic ranges, ~~*IEEE Transactions on Geoscience and Remote Sensing*~~*IEEE Trans. Geosci. Remote Sens.* **41**, 2003, 2674–2677, https://doi.org/10.1109/TGRS.2003.818464.

Cohen J.J, A coefficient of agreement for nominal scales, ~~*Educational and Psychological Measurement*~~*Educ. Psychol. Meas.* **20**, 1960, 37–46, https://doi.org/10.1177/001316446002000104.

De Musso ~~N. M.~~N.M., Capolongo D., Refice A., Lovergine ~~F. P.~~F.P., D'Addabbo A. and Pennetta L., Spatial evolution of the December 2013 Metaponto plain (Basilicata, Italy) flood event using multi-source and high-resolution remotely sensed data, *J. Maps* **14** (2), 2018, 219–229, https://doi.org/10.1080/17445647.2018.1454349.

Deledalle C.-A., Denis L., Tupin F., Reigber A. and Jager M., NL-SAR: a unified nonlocal framework for resolution-preserving (pol)(In)SAR Denoising, ~~*IEEE Transactions on Geoscience and Remote Sensing*~~*IEEE Trans. Geosci. Remote Sens.* **53**, 2015, 2021–2038, https://doi.org/10.1109/TGRS.2014.2352555.

Faccini F., Paliaga G., Piana P., Sacchini A. and Watkins C., The Bisagno stream catchment (Genoa, Italy) and its major floods (1822, 1970 and 2014): geomorphic and land use variations in the last three centuries, *Geomorphology* **273**, 2016, 14–27.

Genidounias ~~Th. D.~~Th.D., Review of the hydraulic works in Serres and Drama Plains, In: *The Exploitation of the Reclaimed Land, after the Productive Projects, in Macedonia,* 1935, Internal report to the Supreme Economic Council of Greece; Athens.

Grimaldi S., Li Y., Pauwels V.R.N. and Walker J.P., Remote sensing-derived water extent and level to constrain hydraulic flood forecasting models: opportunities and challenges, *Surv. Geophys.* **37** (5), 2016, 977–1034, https://doi.org/10.1007/s10712-016-9378-y 232 10.

Groppelli B., Soncini A., Bocchiola D. and Rosso R., Evaluation of future hydrological cycle under climate change scenarios in a mesoscale Alpine watershed of Italy, *NHESS* **11**, 2011, 1769–1785.

Matgen P., Corato G., Chini M., Hostache R. and Giustarini L., Improved flood ~~forcasting~~ forecasting through the assimilation of SAR-derived flood probability maps into 2D hydrodynamic model, In: *IEEE Proc. IGARSS 2015, July 26–31, Milan (Italy),* 2015.

Matgen P., Giustarini L., Chini M., Hostache R., Wood M. and Schlaffer S., Creating a water depth map from SAR flood extent and topography data, In: *IEEE Proc. IGARSS 2016, July 10--15, Beijing, China,* 2016.

Matthews G.V.T., The Ramsar Convention on Wetlands: its History and Development, 1993, Ramsar Convention Secretariat; Gland, Switzerland.

Migliavacca G., Confortola A., Soncini G., Diolaiuti A., Smiraglia C., Barcaza G. and Bocchiola D., Hydrology and potential climate changes in the Rio Maipo (Chile), physical geography and quaternary dynamics, *GFDQ* **38** (2), 2015, 155–168.

Papafilippou-Pennou E., Dynamic Evolution and Recent Exogenic Processes of Strymon River Network in Serres Graben, PhD Thesis, **243**, 2004, School of Geology, Aristotle University of Thessaloniki; Thessaloniki, Greece.

Pulvirenti L., Pierdicca N., Boni G., Fiorini M. and Rudari R., Flood damage assessment through multitemporal COSMO-SkyMed data and hydrodynamic models: the Albania 2010 case study, *IEEE J. Sel. Top. Appl. Earth Obs. Remote Sens.* **7** (7), 2014, 2848–2855, https://doi.org/10.1109/JSTARS.2014.2328012.

Refice A., Capolongo D., Pasquariello G., D'Addabbo A., Bovenga F., Nutricato R., Lovergine F.P. and Pietranera L., SAR and InSAR for flood monitoring: examples with COSMO- SkyMed data, *IEEE J. Sel. Top. Appl. Earth Obs. Remote Sens.* **7** (7), 2014, 2711–2722, https://doi.org/10.1109/JSTARS.2014.2305165.

Refice A., D'Addabbo A. and Capolongo D., (Eds.), *Flood Monitoring through Remote Sensing,* 2018a, Springer.

Refice A., D'Addabbo A. and Capolongo, Methods, techniques and sensors for precision flood monitoring Through remote sensing, In: *Flood Monitoring through Remote Sensing,* 2018b, Springer; Cham, 1–25.

Refice A., D'Addabbo A., Lovergine F.P., Tijani K., Morea AA., Nutricato R., Bovenga F. and Nitti D.O., Monitoring flood extent and area through multisensor, multi-temporal remote sensing: the Strymonas (Greece) river flood, In: *Flood Monitoring through Remote Sensing,* 2018c, Springer International Publishing, 101–113, https://doi.org/10.1007/978-3-319-63959-8_5.

Righini M. and Surian N., Remote sensing as a tool for analysing channel dynamics and geomorphic effects of floods, In: *Flood Monitoring through Remote Sensing,* 2018, Springer; Cham, 27–59.

Rinaldo AA., Bertuzzo EE., Mari LL., Righetto LL., Blokesch MM., Gatto MM., Casagrandi RR., Murray MM., Vesenbeckh SMS.M. and Rodriguez-Iturbe I., Reassessment of the 2010–2011 Haiti cholera outbreak and rainfall-driven multiseason projections, *PNAS* **109** (17), 2012, 6602–6607.

Schreier G., (Ed), *SAR Geocoding: Data and Systems,* 1993, (Wichmann).

Schumann G.J.P., Bates P.D., Horritt M.S., Matgen P. and Pappenberger F., Progress in integration of remote sensing-derived flood extent and stage data and hydraulic models, *Rev. Geophys.* **47** (3), 2009, , RG4001https://doi.org/10.1029/2008RG000274.

Soncini A., Bocchiola D., Confortola G., Minora U., Vuillermoz E., Salerno F., Viviano G., Shrestha D., Senese A., Smiraglia C. and Diolaiuti G., Future hydrological regimes and glacier cover in the Everest region: the case study o the Dudh Koshi basin, *Sci. Total Environ.* **565**, 2016, 1084–1101.

Soncini A., Bocchiola D., Azzoni R.S. and Diolaiuti G., A methodology for monitoring and modeling of high altitude Alpine catchments, *Progress in Physical GeographyProg. Phys. Geogr.* **41** (4), 2017, 393–420.

Vouvalidis K., Morphological, Sedimentological, Oceanographic Processes and Human Impacts Contributing to the Evolution of Strymonas River, 1998, Aristotle University of Thessaloniki, Thessaloniki, Greece; PhD Dissertation.

Graphical abstract

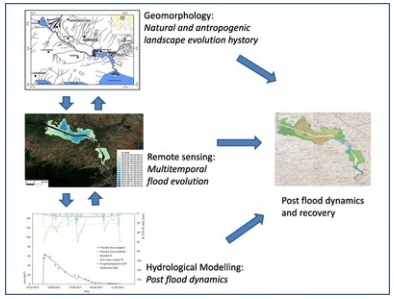

alt-text: Unlabelled Image

Highlights

- Geomorphological ~~hystory~~ history of the Strymonas river basin controls spatial flood inundation.
- Multitemporal satellite images allowed ~~to retrieve~~ retrieving several inundation maps at different times.
- Simplified hydrological modeling allowed ~~-~~ inference about long-term dynamics of flooded areas.
- Integration of geomorphology, remote sensing and hydrological modeling allowed ~~to reconstruct~~reconstructing post flood dynamics.

Queries and Answers

Query:

Your article is registered as a regular item and is being processed for inclusion in a regular issue of the journal. If this is NOT correct and your article belongs to a Special Issue/Collection please contact p.das@elsevier.com immediately prior to returning your corrections.

Answer: Yes

Query:

Please confirm that given names and surnames have been identified correctly and are presented in the desired order, and please carefully verify the spelling of all authors' names.

Answer: correct author spelling : Stamatopoulos

Query:

The author names have been tagged as given names and surnames (surnames are highlighted in teal color). Please confirm if they have been identified correctly.

Answer: Yes

Query:

Affiliation "5" is not linked to any author in the original manuscript; hence, we have opted to link this affiliation to the first author. Please check and provide changes as necessary.

Answer: No the n. 5 affiliation must be linked to Stamatopoulos instead of 3. And not to the first author.

Query:

Citation "Wood et al. (2016)" has not been found in the reference list. Please supply full details for this reference.

Answer: Wood M, Hostache R, Neal J, Wagener T, Giustarini L, Chini M, Corato G, Matgen P, Bates P. Calibration of channel depth and friction parameters in the LISFLOOD-FP hydraulic model using medium-resolution SAR data and identifiability techniques. Hydrology and Earth System Sciences. 2016 Dec 19;20(12):4983-97.

Query:

This sentence has been slightly modified for clarity. Please check and confirm if the meaning is still correct.

Answer: Yes

Query:

The citation “Groppelli et al., 2011a” has been changed to “Groppelli et al., 2011” to match the author name/date in the reference list. Please check if the change is fine in this occurrence and modify the subsequent occurrences, if necessary.

Answer: yes fine

Query:

Please check the presentation of all equations, and amend if necessary.

Answer: they look fine.

Query:

The citation “Bocchiola et al., 2009” has been changed to “Bocchiola and Rosso, 2009” to match the author name/date in the reference list. Please check if the change is fine in this occurrence and modify the subsequent occurrences, if necessary.

Answer: yes, fine.

Query:

Please note that Fig. 6 was not cited in the text. Please check if the suggested citation is appropriate, and correct if necessary.

Answer: the citation is not correct. Delete. Actually, figure 6 is cited after the the figure where it says: "Figure6shows the DEMheight map" It needs only to be changed in FIG. 6

Query:

Uncited references: This section comprises references that occur in the reference list but not in the body of the text. Please position each reference in the text or, alternatively, delete it. Thank you.

Answer: Please delete

Query:

Have we correctly interpreted the following funding source(s) and country names you cited in your article: "Agenzia Spaziale Italiana, Italy; Japan Aerospace Exploration Agency, Japan".

Answer: Yes